JOURNAL OF GEOPHYSICAL RESEARCH: ATMOSPHERES, VOL. 118, 9351–9366, doi:10.1002/jgrd.50672, 2013

Influence of boundary layer dynamics and isoprene chemistry on the organic aerosol budget in a tropical forest

R. H. H. Janssen,[1,2] J. Vilà-Guerau de Arellano,[3] J. L. Jimenez,[4] L. N. Ganzeveld,[1] N. H. Robinson,[5,6] J. D. Allan,[5,7] H. Coe,[5] and T. A. M. Pugh[8,9]

Received 2 November 2012; revised 2 July 2013; accepted 16 July 2013; published 20 August 2013.

[1] We study the organic aerosol (OA) budget in a tropical forest by analyzing a case that is representative for the OP3 campaign at Borneo. A model is designed that combines the essential dynamical and chemical processes that drive the diurnal evolution of reactants in the atmospheric boundary layer (BL). In this way, the model simultaneously represents the effects and interactions of various dynamical and chemical factors on the OA budget. The model is able to reproduce the observed diurnal dynamics of the BL, including the evolution of most chemical species involved in secondary organic aerosol (SOA) formation. A budget analysis of the contributions of the dynamic and chemical processes reveals the significance of the entrainment process in the diurnal evolution of SOA. Further, we perform a series of sensitivity analyses to determine the effect of meteorological forcings and isoprene chemical pathways on the OA budget. Subsidence and advection of cool air have opposing effects on the OA concentration, although both suppress BL growth. Recycling of the OH radical in the oxidation of isoprene may affect the amount of SOA that is formed, but must be understood better before its impact can be definitely determined. SOA formation from isoprene is calculated for both the low- and high-NO_x pathway, with the latter dominating the isoprene peroxy radical chemistry. Finally, we study the significance of SOA formation through the reactive uptake of isoprene epoxydiols on acidic sulfate aerosol. Despite the incorporation of these new pathways, the OA concentration is systematically underestimated by about a factor of 2.

Citation: Janssen, R. H. H., J. Vilà-Guerau de Arellano, J. L. Jimenez, L. N. Ganzeveld, N. H. Robinson, J. D. Allan, H. Coe, and T. A. M. Pugh (2013), Influence of boundary layer dynamics and isoprene chemistry on the organic aerosol budget in a tropical forest, *J. Geophys. Res. Atmos.*, *118*, 9351–9366, doi:10.1002/jgrd.50672.

[1]Earth System Science and Climate Change, Wageningen University and Research Center, Wageningen, Netherlands.
[2]Now at Atmospheric Chemistry Department, Max Planck Institute for Chemistry, Mainz, Germany.
[3]Meteorology and Air Quality Section, Wageningen University and Research Center, Wageningen, Netherlands.
[4]Cooperative Institute for Research in the Environmental Sciences and Department of Chemistry and Biochemistry, University of Colorado Boulder, Boulder, Colorado, USA.
[5]Centre for Atmospheric Science, School of Earth Atmospheric and Environmental Science, University of Manchester, Manchester, UK.
[6]Now at Seasonal to Decadal Prediction, The Met Office, Exeter, United Kingdom.
[7]National Centre for Atmospheric Science, The University of Manchester, Manchester, UK.
[8]Lancaster Environment Centre, University of Lancaster, Lancaster, UK.
[9]Now at Karlsruhe Institute of Technology, Institute of Meteorology and Climate Research/Atmospheric Environmental Research (IMK-IFU), Garmisch-Partenkirchen, Germany.

Corresponding author: R. H. H. Janssen, Atmospheric Chemistry Department, Max Planck Institute for Chemistry, Hahn-Meitner-Weg 1, Mainz, D-55128, Germany. (ruud.janssen@mpic.de)

2169-897X/13/10.1002/jgrd.50672

1. Introduction

[2] Tropical forests are potentially an important source of biogenic secondary organic aerosol (SOA), due to high emissions of isoprene and terpenes [*Langford et al.*, 2010; *Karl et al.*, 2007] and potentially high concentrations of their most important oxidant, the hydroxyl radical (OH) [*Lelieveld et al.*, 2008]. Recently, a number of measurement campaigns have been conducted to gain insight in the sources and formation mechanisms of SOA in forests in Amazonia (AMAZE) [*Chen et al.*, 2009], West-Africa (AMMA) [*Capes et al.*, 2009], and South-East Asia (OP3) [*Robinson et al.*, 2011a, 2011b, 2012]. When interpreting observations made in the atmospheric boundary layer (BL) during these campaigns, it is important to realize that the evolution of chemical species in the BL is a function of chemical conversion, emission/deposition, advection, and the vertical exchange of compounds between the free troposphere (FT) and the BL driven by entrainment [*Vilà-Guerau de Arellano et al.*, 2009; *Ouwersloot et al.*, 2012] and gas/particle partitioning in case of SOA. In addition, subsidence and advection of heat and moisture influence the

growth of the BL and therefore modify its dilution capacity and the exchange of species between the BL and FT, as controlled by entrainment [*Ouwersloot et al.*, 2012]. Here we investigate the diurnal budget of OA by combining a model that reproduces the diurnal variability of the dynamics and chemistry of the BL with observations from the OP3 campaign.

[3] There is still a considerable gap between the understanding of ambient biogenic SOA and the ability of models to reproduce its observed concentration. Simulations by both *Capes et al.* [2009] and *Chen et al.* [2009] underpredicted SOA concentrations in isoprene-dominated tropical environments, but these studies could not rule out the possibility of canceling errors, due to the limited observational constraints on these estimates. These sources of uncertainty were the identification and emission rates of biogenic SOA precursors, SOA formation mechanisms, oxidant concentrations, the SOA particle mass yields, the influence of vertical mixing and advection, and the unknown contribution of the background OA concentration (OA_{BG}). On the other hand, *Slowik et al.* [2010] were able to reproduce observed OA concentrations in a rural environment dominated by terpene emissions. *Sjostedt et al.* [2011], however, underestimated OA compared to the measurements in an environment where isoprene was more abundant, both using the same model as *Slowik et al.* [2010] and an approach based on VOC destruction rates.

[4] The underestimation of modeled OA in environments with high isoprene emissions may be due to a lack of understanding of the chemical pathways that lead to the formation of SOA from isoprene (ISOA). Current parameterizations of ISOA formation are therefore subject to large uncertainties [*Carlton et al.*, 2009]. More specifically, *Surratt et al.* [2010] suggested that peroxy methacryloyl nitrate (MPAN) and isoprene epoxydiols (IEPOX) are important intermediate gas-phase species for SOA formation under high- and low-NO_x conditions, respectively. The mechanisms of SOA formation through these reaction pathways have only recently started to be explored [*Paulot et al.*, 2009; *Surratt et al.*, 2010; *Chan et al.*, 2010; *Lin et al.*, 2012b; *Kjaergaard et al.*, 2012].

[5] Another issue related to isoprene chemistry in tropical forests is the mismatch between measurements and theoretical calculations of OH concentrations, which has been attributed to regeneration of OH in the oxidation of isoprene [*Lelieveld et al.*, 2008]. Several mechanistic pathways leading to OH recycling have been proposed, but none of them has been able to explain the gap between measurements and models [*Stone et al.*, 2011]. *Taraborrelli et al.* [2012] recently formulated a detailed mechanism for isoprene oxidation by assembling and completing several previously proposed mechanisms, with which they were able to reproduce OH concentrations under pristine tropical conditions to within the bounds of the measurement uncertainty. In their mechanism, unsaturated hydroperoxyaldehydes (HPAL) that are formed in the oxidation of isoprene play a central role, as HPAL photolysis initiates a reaction cascade that results in OH production. The net production or loss of OH is the result of the competition between this OH production and its consumption by HPAL. Another point of view was presented by *Mao et al.* [2012], who suggested that the high observed OH concentrations

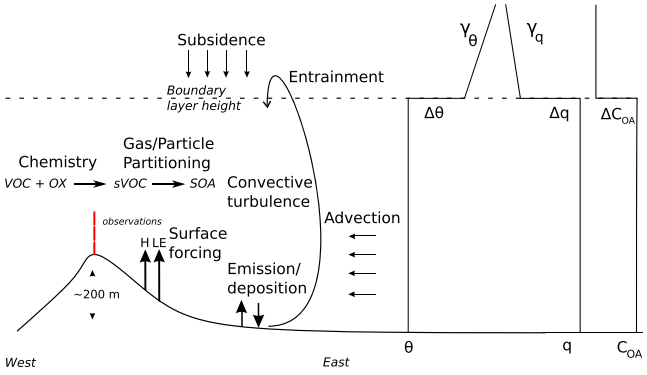

Figure 1. Conceptual representation of the main dynamic and chemical contributions to the organic aerosol budget during the OP3 campaign and sketches of typical vertical profiles of potential temperature (θ), specific humidity (q), and organic aerosol concentration (C_{OA}).

may be the result of a measurement artifact. Their findings, however, are very much dependent on instrument design and environmental conditions. The effect of OH recycling on SOA formation has so far been subject of only one study [*Lin et al.*, 2012a], and it is still unclear how the formation of ISOA-forming products depends on OH concentrations [*Carlton et al.*, 2009].

[6] The OP3 campaign provides a challenging case since the aerosol at Borneo is influenced by complex terrain and multiple sources. The measurement tower is located on top of a 200 m hill, which means that it could be influenced by anabatic flows, which are upslope flows driven by heating of the slope by insolation [e.g., *Thunis and Bornstein*, 1996]. The proximity of the coast means that the site may be influenced by sea breeze circulations [*Robinson et al.*, 2012] and heterogeneities at smaller spatial scales can induce advection of heat, moisture, and chemical species [*Ouwersloot et al.*, 2011]. Moreover, the aerosol has multiple sources: *Robinson et al.* [2012] investigated the effect of the island on the vertical distribution of aerosol through the troposphere, based on aircraft observations and showed that air is enriched in OA as it passes over the island, which indicates a large on-island source of biogenic SOA. An analysis of air mass back trajectories for the site based on European Centre for Medium-Range Weather Forecasts (ECMWF) wind fields, however, revealed that during the campaign, there was no period during which the rain forest was the only source of aerosol and that significant levels of (off-island) sulfate aerosol were transported to the site [*Robinson et al.*, 2011b]. This is in contrast with the Amazon, which experiences periods with predominant in-basin influences during which biogenic SOA dominates the aerosol mass [*Chen et al.*, 2009].

[7] Extending on the work of *Robinson et al.* [2011b, 2012], we focus on the interpretation of ground-based OA measurements made during OP3 and how various dynamic and chemical terms contribute to the organic aerosol budget. A schematic overview of these factors is presented in Figure 1. We aim for an integrated approach by simultaneously accounting for atmospheric boundary layer processes, as influenced by local surface and large-scale meteorological forcings, and for chemical processes, related to both

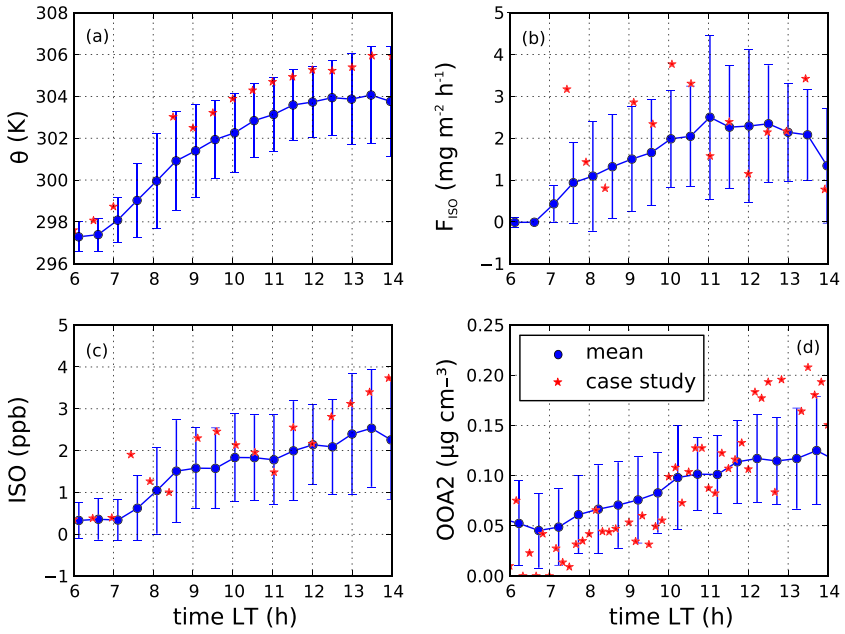

Figure 2. Campaign mean and case study diurnal evolution of measured (a) potential temperature (θ), (b) isoprene emission flux (F_{ISO}), (c) isoprene concentration (ISO), and (d) concentration of the SV-OOA factor (OOA2). The error bars indicate the standard deviation.

gas-phase and secondary aerosol chemistry and partitioning. In our study, we overcome some of the issues in previous studies of the OA budget in tropical forests by prescribing VOC emissions as constrained by above-canopy flux measurements, by accounting for entrainment, including its interaction with subsidence and advection of heat, and by performing an experiment in which OH concentrations are matched with observations by including OH regeneration in isoprene oxidation in the model. Since this case is well constrained with data, it gives the opportunity to assess which processes contribute most to these large uncertainties, and we shed some light on some other factors that are not that well constrained and are yet uncertain or difficult to estimate, for example subsidence.

[8] To this end, we use MXLCH-SOA, a 0-D model that reproduces the essentials of the dynamics of the convective boundary layer, the gas-phase chemistry leading to the formation of semivolatile organics and the gas/particle partitioning of these organic species [*Janssen et al.*, 2012]. In the design of the model, we have kept a balance between the level of complexity of the representations of the different components, and its ability to reproduce the observations of dynamics and chemistry. In this way, MXLCH-SOA allows us to break down the budgets of OA and its precursors into the various dynamical and chemical terms that contribute to them. To carry out the current study, we implement a representation of SOA formation from isoprene using the volatility basis set (VBS) approach. After examining the complete data set, we select a representative case study, discuss the performance of the model when compared to the case study observations and show the contributions of several factors to the budget of OA and its precursors. Then, we analyze the impact of large-scale meteorological forcings on the OA concentration, discuss the potential role of OH recycling in SOA formation, and analyze the formation of SOA from IEPOX. The latter has been suggested to yield a specific tracer (hereinafter called 82Fac) [*Lin et al.*, 2012b] that is present in the OA observed by an aerosol mass spectrometer (AMS) at Borneo [*Robinson et al.*, 2011a].

2. Methods

2.1. Observations of the Diurnal Variability During OP3

[9] Data gathered during the OP3 campaign enable us to study the diurnal variation of atmospheric compounds modulated by surface and BL processes. OP3 was conducted in Malaysia in 2008 [*Hewitt et al.*, 2010], and here we use data from OP3 III (23 June to 20 July) at the Bukit Atur Global Atmospheric Watch station, located in the Danum Valley rain forest conservation area in Sabah, Borneo (4°58′ N, 117°50′ E, 426 m above sea level). The site was located in a clearing at the top of a 200 m hill, above most of the surrounding forest. The observations were made from a measurement tower of 100 m on top of this hill, and measurement heights in this paper are indicated as height relative to the base of the tower. Figure 1 shows a schematic overview of the measurement setting and processes that potentially influence the formation and evolution of local OA. Note that we only study processes that are occurring in the daytime convective boundary layer, i.e., the well-mixed layer above the canopy. The measurements of both fluxes and concentrations that we use to constrain our model are all taken above the canopy layer.

[10] Figure 2 shows mean diurnal cycles during OP3 III, based on half-hourly averages over a period of 4 weeks.

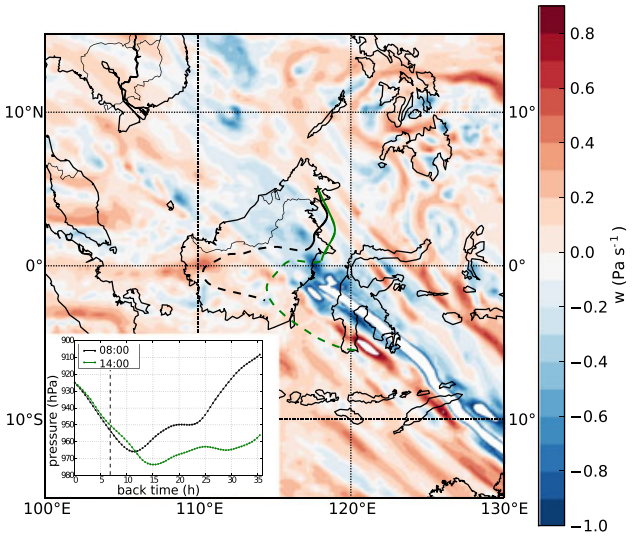

Figure 3. Vertical wind speed w at 850 hPa at 14:00 LT on 7 July 2008 and 120 (dashed lines) and 36 h (solid lines) air mass back trajectories arriving at Bukit Atur at 08:00 (black) and 14:00 (green), respectively, at a pressure altitude of 925 hPa. Note that positive values of vertical wind speed reflect subsidence, since it is expressed in units of pressure. Both are based on ECMWF wind fields with a resolution of 1.125° · 1.125°. The inset shows the pressure level of the back trajectories with the dotted line indicating their approximate arrival time over land.

It includes the most representative dynamic, surface, and chemistry variables, as represented by potential temperature (θ), isoprene flux (F_{ISO}), isoprene concentration (ISO), and concentration of OOA2, an oxidized organic aerosol (OOA) factor, respectively. θ rises during the day due to the sensible heat flux and entrainment of warm air, F_{ISO} follows a diurnal cycle driven by temperature and light intensity [*Langford et al*., 2010], ISO follows F_{ISO} but is also modified by chemical transformations and BL dynamics, and the full complexity of the behavior of OOA2 is under study here.

[11] We selected one representative day for which we initialize and evaluate the diurnal evolution of chemistry and dynamics of our model with observations: 7 July 2008. To determine the representativeness of this specific day for a typical day at the measurement site during OP3 III, we compared observations from this day to the campaign mean (Figure 2). Similar diurnal trends are present in the data of the case study and in the campaign averages. Additionally, the observations from the case study fall within the standard deviation of these averages, except for OOA2 in the afternoon.

[12] Furthermore, the selection of this day is based on the relatively smooth evolution of the surface heat fluxes during this day, which ensures convection and turbulent mixing occurring throughout the BL. Additionally, the observed diurnal cycle of the ozone photolysis rate jO^1D followed the theoretical clear-sky diurnal evolution relatively smoothly compared to other days during the campaign, although there were some fluctuations, probably caused by clouds. These conditions were valid until ∼14:00 LT. After 14:00, temperature dropped drastically and also moisture and concentrations of chemical species suddenly changed. Possible explanations for such behavior are the formation of clouds or the arrival of the sea breeze at the site. To avoid the complex transport and chemistry associated with the presence of clouds on top of the BL, we finalize our analysis at 14:00 and focus on the period with strong boundary layer growth and OA formation. The validity of the assumption of a well-mixed layer during this day is further supported by vertical profiles of O_3 and NO_x, which were obtained by measuring these species at several heights between 5 and 75 m (not shown). Especially from 45 m upward, O_3 and NO_2 measurements are very similar at different heights, indicating that above this height, we are probing mixing ratios within the BL. On the other hand, this means that observations below 45 m could be in the surface layer and may therefore deviate from mixed layer values.

[13] Finally, an important reason for the selection of this day is the availability of the most complete data set of dynamics, gas-phase chemistry (most importantly VOCs and oxidants), and OA. Upper air observations of OA concentrations are potentially very useful for understanding the evolution of OA in the BL [*Janssen et al.*, 2012]. While several vertical profiles of OA over the measurement site have been obtained, unfortunately, no flight was carried out on this particular day [*Robinson et al.*, 2012]. Therefore, we use observations from other days to get an estimate of FT OA concentrations.

[14] On 7 July 2008, the measurement site was influenced by air masses arriving from the South-East (Figure 3), which means that the air masses were affected by substantial amounts of both off-island and on-island emissions. Consequently, they contained sulfate aerosol from off-island sources and were affected by isoprene emissions from oil palm plantations located to the South-East of the observational site (see *Hewitt et al.* [2010] for a detailed land-use map). The air masses traveled about 7 h over land before arriving at the measurement site. The pressure altitude during the period over land indicates that the air masses were close to the surface and within the BL. An additional meteorological factor important for our research is the presence of subsiding air motions. The site and its surroundings were influenced by subsidence, as can be inferred from ECMWF reanalysis fields of vertical velocity at the 850 hPa level (Figure 3). The downward movement of air with 0.2 Pa s^{-1} over Bukit Atur corresponds with a vertical velocity of –2 cm s^{-1}.

2.2. Description of MXLCH-SOA

[15] The MXLCH-SOA model is based on mixed layer (MXL) theory [*Lilly*, 1968; *Tennekes*, 1973; *Vilà-Guerau de Arellano et al.*, 2009, 2011], which states that under convective conditions, strong turbulent mixing causes perfect mixing of quantities over the entire depth of the BL. Therefore, scalars and reactants in the convective boundary layer are characterized by a single value over the whole depth of the BL. The BL dynamics are driven by the surface heat fluxes that are prescribed to the model. The buoyancy entrainment flux is parameterized by a zeroth-order closure assumption in which the entrainment flux is a fixed fraction (β) of the surface buoyancy flux (Table 3). In addition, large-scale meteorological forcings that influence the BL dynamics, like subsidence caused by high pressure sys-

Table 1. Chemical Reaction Scheme Used in the Numerical Experiments With MXLCH-SOA[a]

Number	Reaction	Reaction Rate
R1	$O_3 + h\nu \rightarrow O^1D + O_2$	$3.00 \cdot 10^{-5} \cdot e^{\frac{-0.575}{\cos(\chi)}}$
R2	$O^1D + H_2O \rightarrow 2OH$	$1.63 \cdot 10^{-10} \cdot e^{\frac{60}{T}}$
R3	$O^1D + N_2 \rightarrow O_3$	$2.15 \cdot 10^{-11} \cdot e^{\frac{110}{T}}$
R4	$O^1D + O_2 \rightarrow O_3$	$3.30 \cdot 10^{-11} \cdot e^{\frac{55}{T}}$
R5	$NO_2 + h\nu \rightarrow NO + O_3$	$1.67 \cdot 10^{-2} \cdot e^{\frac{-0.575}{\cos(\chi)}}$
R6	$CH_2O + h\nu \rightarrow HO_2$	$1.47 \cdot 10^{-4} \cdot e^{\frac{-0.575}{\cos(\chi)}}$
R7	$OH + CO \rightarrow HO_2$	$2.40 \cdot 10^{-13}$
R8	$OH + CH_4 \rightarrow CH_3O_2$	$2.45 \cdot 10^{-12} \cdot e^{\frac{-1775}{T}}$
R9	$\mathbf{OH + ISO} \rightarrow IRO_2 + \alpha_1^I\mathbf{IC}_1 + \alpha_2^I\mathbf{IC}_2 + \alpha_3^I\mathbf{IC}_3$	$2.70 \cdot 10^{-11} \cdot e^{\frac{390}{T}}$
R10	$OH + [MVK+MACR] \rightarrow HO_2 + CH_2O$	$2.40 \cdot 10^{-11}$
R11	$OH + HO_2 \rightarrow H_2O + O_2$	$4.80 \cdot 10^{-11} \cdot e^{\frac{250}{T}}$
R12	$OH + H_2O_2 \rightarrow H_2O + HO_2$	$2.90 \cdot 10^{-12} \cdot e^{\frac{-160}{T}}$
R13	$HO_2 + O_3 \rightarrow OH + 2O_2$	$2.03 \cdot 10^{-16} \cdot (\frac{T}{300})^{4.57} e^{\frac{693}{T}}$
R14	$HO_2 + NO \rightarrow OH + NO_2$	$3.50 \cdot 10^{-12} \cdot e^{\frac{250}{T}}$
R15	$CH_3O_2 + NO \rightarrow HO_2 + NO_2 + CH_2O$	$2.80 \cdot 10^{-12} \cdot e^{\frac{300}{T}}$
R16	$IRO_2 + NO \rightarrow HO_2 + NO_2 + 0.6[MVK + MACR] + CH_2O$	$1.00 \cdot 10^{-11}$
R17	$OH + CH_2O \rightarrow HO_2 + CO$	$5.50 \cdot 10^{-12} \cdot e^{\frac{125}{T}}$
R18	$2HO_2 \rightarrow H_2O_2 + O_2$	*
R19	$CH_3O_2 + HO_2 \rightarrow PRODUCTS$	$4.10 \cdot 10^{-13} \cdot e^{\frac{750}{T}}$
R20	$IRO_2 + HO_2 \rightarrow n\,OH + PRODUCTS$	$1.50 \cdot 10^{-11}$
R21	$OH + NO_2 \rightarrow HNO_3$	$3.50 \cdot 10^{-12} \cdot e^{\frac{340}{T}}$
R22	$NO + O_3 \rightarrow NO_2 + O_2$	$3.00 \cdot 10^{-12} \cdot e^{\frac{-1500}{T}}$
R23	$NO + NO_3 \rightarrow 2NO_2$	$1.80 \cdot 10^{-11} \cdot e^{\frac{110}{T}}$
R24	$NO_2 + O_3 \rightarrow NO_3 + O_2$	$1.40 \cdot 10^{-13} \cdot e^{\frac{-2470}{T}}$
R25	$NO_2 + NO_3 \rightarrow N_2O_5$	**
R26	$N_2O_5 \rightarrow NO_3 + NO_2$	***
R27	$N_2O_5 + H_2O \rightarrow 2HNO_3$	$2.50 \cdot 10^{-22}$
R28	$N_2O_5 + 2H_2O \rightarrow 2HNO_3 + H_2O$	$1.80 \cdot 10^{-39}$
R29	$\mathbf{TERP + O_3} \rightarrow \alpha_1^T\mathbf{TC}_1 + \alpha_2^T\mathbf{TC}_2 + \alpha_3^T\mathbf{TC}_3 + \alpha_4^T\mathbf{TC}_4$	$5.00 \cdot 10^{-16} \cdot e^{\frac{-530}{T}}$
R30	$\mathbf{TERP + OH} \rightarrow \alpha_1^T\mathbf{TC}_1 + \alpha_2^T\mathbf{TC}_2 + \alpha_3^T\mathbf{TC}_3 + \alpha_4^T\mathbf{TC}_4$	$5.00 \cdot 10^{-16} \cdot e^{\frac{-530}{T}}$

*$k = (k1 + k2)/k3;\ k1 = 2.21 \cdot 10^{-13} \cdot e^{\frac{600}{T}};\ k2 = 1.91 \cdot 10^{-33} \cdot e^{\frac{980}{T}} \cdot c_{\mathrm{air}};\ k3 = 1 + 1.4 \cdot 10^{-21} \cdot e^{\frac{2200}{T}} \cdot c_{H_2O}$

**$k = 0.35 \cdot (k_0 k_\infty)/(k_0 + k_\infty);\ k_0 = 3.61 \cdot 10^{-30} \left(\frac{T}{300}\right)^{-4.1} \cdot c_{N_2};\ k_\infty = 1.91 \cdot 10^{-12} \left(\frac{T}{300}\right)^{0.2}$

***$k = 0.35 \cdot (k_0 k_\infty)/(k_0 + k_\infty);\ k_0 = 1.31 \cdot 10^{-3} \left(\frac{T}{300}\right)^{-3.5} \cdot e^{\frac{-11000}{T}} \cdot c_{N_2};\ k_\infty = 9.71 \cdot 10^{14} \left(\frac{T}{300}\right)^{0.1} \cdot e^{\frac{-11080}{T}}$

[a]In the reaction rates, T is the absolute temperature in Kelvin and χ is the solar zenith angle. First-order reaction rates are in s^{-1}, second-order reaction rates in cm^3 molecule^{-1} s^{-1}. Aerosol-forming reactions and products are printed in bold font. α_1^I–α_4^I and α_1^T–α_4^T are the stoichiometric coefficients for ISO and TERP, respectively, see Table 2. In R20, n is the rate of OH recycling, PRODUCTS are the species which are not further evaluated in this chemical reaction scheme. Reaction of isoprene with O_3 is not considered.

tems and advection of heat and moisture, are prescribed to the model as external forcings. The transition between the well-mixed BL and the free troposphere is marked by an infinitesimally thin inversion layer. Typical profiles of potential temperature, specific humidity, and OA are shown in Figure 1. The complete MXL equations are given by *Vilà-Guerau de Arellano et al.* [2009] and *Ouwersloot et al*. [2012].

[16] It is coupled to a reduced chemistry scheme which contains the essentials of the O_3-NO_x-VOC-HO_x system [*Vilà-Guerau de Arellano et al.*, 2011] and a module for gas/particle partitioning using the VBS approach [*Donahue et al.*, 2006]. At each time step, the total organic aerosol concentration C_{OA} is calculated from:

$$C_{\mathrm{OA}} = \sum_i (X_{p,i} C_i) + \mathrm{OA_{BG}}\,; \quad X_{p,i} = \left(1 + \frac{C_i^*}{C_{\mathrm{OA}}}\right)^{-1}, \qquad (1)$$

where C_{OA} is the organic aerosol mass concentration ($\mu g\,m^{-3}$), $X_{p,i}$ is the fraction of semivolatile compound i in the aerosol phase (dimensionless), C_i is the concentration of the semivolatile organic compound (SVOC), originating from isoprene (IC_i) or terpene (TC_i) ($\mu g\,m^{-3}$), OA_{BG} is the background organic aerosol concentration ($\mu g\,m^{-3}$), which is assumed to be nonvolatile, and C_i^* is the effective saturation concentration of compound i ($\mu g\,m^{-3}$).

[17] SOA formation from isoprene is implemented in two ways. In the default mechanism, as used in the base case, SVOCs originate directly from first-step oxidation of isoprene by OH (Table 1) using yields derived from lab studies [*Kroll et al.*, 2006], which is common practice in air quality models [e.g., *Slowik et al.*, 2010; *Tsimpidi et al.*, 2010]. Oxidation of isoprene by OH produces both the SVOC species IC_i and IRO_2, an isoprene peroxy radical, which further influences the gas-phase chemistry and therewith OH regeneration. IC_i partition into the aerosol phase, together with the SVOCs formed from terpene oxidation (TC_i). The only difference between the isoprene and terpene oxidation products is their molecular weight (136 and 180 g mol^{-1}, respectively). The SVOC yields strongly depend on NO_x concentrations, and we account for this by linearly interpolating the high and low NO_x yields (Table 2) as a function

Table 2. Stoichiometric Coefficients at $T = 298$ K for the Different Volatility Bins of the SOA Precursor Categories TERP and ISO, With Saturation Concentration C_i^* in $\mu g\ m^{-3}$ From *Tsimpidi et al*. [2010]

i	1	2	3	4
C_i^*	1	10	100	1000
TERP, low-NO_x	0.107	0.092	0.359	0.600
TERP, high-NO_x	0.012	0.122	0.201	0.500
ISO, low-NO_x	0.009	0.030	0.015	–
ISO, high-NO_x	0.001	0.023	0.015	–

of the branching of the reaction of RO_2 from isoprene and terpenes through the NO and the HO_2 channel, respectively [*Lane et al.*, 2008].

[18] In the default mechanism, we omit the formation of IEPOX of which markers are present in the OA at the site [*Robinson et al.*, 2011a; *Lin et al.*, 2012b]. In a sensitivity analysis, we include a first-order estimate of ISOA from this pathway, which is thought to be the dominant source of ISOA under low-NO_x conditions [*Surratt et al.*, 2010].

[19] Under high-NO_x conditions, MPAN is an important intermediate species in ISOA formation. Although IRO_2 mainly reacts with NO under the conditions of this study, we have not included formation of ISOA though MPAN in our model. MPAN is formed when the NO_2/NO ratio is high [*Chan et al.*, 2010], which is not the case here and likely also in other tropical regions. Furthermore, MPAN decomposes at temperatures higher than 15°C (D. R. Worton et al., Observational constraints on high- and low-NO_x aerosol formation from isoprene, submitted to *Environmental Science and Technology*, 2013) and is therefore probably not an important SOA precursor under the temperature range during our case study, with temperatures above 25°C. In future studies, MXLCH-SOA could be used to evaluate the performance of more detailed ISOA-forming mechanisms under high- and low-NO_x to test the validity of these assumptions.

[20] In our reduced chemical mechanism (Table 1), the gas-phase oxidation of isoprene is highly simplified and all first-generation products of isoprene oxidation are lumped into a single species, which combines methyl vinyl ketone and methacrolein (MVK+MACR). Together, they have a yield of 60% [e.g., *Karl et al.*, 2009]. In the comparison with observations, it is important to note that in the PTR-MS measurements that we use here, MVK and MACR are also observed as one lumped species, since they have the same molecular weight.

2.3. Initialization of MXLCH-SOA

[21] Initial and boundary conditions are obtained by fitting MXLCH-SOA to the case study observations of dynamics and chemistry, thereby constituting the base case upon which further experiments are based. The initial OA_{BG} in the BL is taken as the total OA concentration, as derived from AMS measurements [*Robinson et al.*, 2011a]. An initial BL concentration of 0.60 $\mu g\ m^{-3}$ is obtained, consisting of 0.04 $\mu g\ m^{-3}$ OOA2, a semivolatile oxidized organic aerosol (OOA) factor, 0.06 $\mu g\ m^{-3}$ 82Fac, a factor attributed to IEPOX SOA, 0.30 $\mu g\ m^{-3}$ OOA1, a low-volatile OOA factor, and 0.20 $\mu g\ m^{-3}$ 91Fac, an OA factor associated with biomass burning [*Robinson et al.*, 2011a, 2011b]. The OA_{BG} in the FT is also set to 0.60 $\mu g\ m^{-3}$, i.e., BL OA_{BG} = FT OA_{BG}. Vertical profiles of OA obtained from aircraft observations support the assumption that OA concentrations in the FT over East Borneo can be at most equal to the OA concentrations in the BL, but not higher [*Robinson et al.*, 2012]. Since entrainment does not dilute the modeled OA_{BG} when concentrations in BL and FT are equal (see equation (5)), this is the most favorable assumption for calculated OA concentrations in the BL.

[22] Dry deposition has been suggested to be an important sink for oxidized VOCs [*Karl et al.*, 2010] and consequently to decrease SOA production significantly [*Bessagnet et al.*, 2010]. Therefore, we included it by applying a deposition velocity of 2.4 cm s^{-1} for MVK+MACR and for all SVOCs, which is the above-canopy deposition velocity for MVK+MACR as found in flux measurements in the Amazon [*Karl et al.*, 2010]. *Pugh et al.* [2010] found that such a large deposition velocity is needed to reconcile modeled MVK+MACR concentrations with measurements. For SVOCs, the V_d of 2.4 cm s^{-1} is taken as an upper limit as not every SVOC will be as effectively taken up and metabolized as MVK+MACR [*Karl et al.*, 2010]. Since the actual deposition velocity for SVOCs is uncertain, we included a simulation in which their deposition is switched off ($V_d = 0$). In this way, we obtain an upper and a lower limit for the effect of dry deposition of SVOCs.

2.4. Numerical Experiments

[23] A set of numerical experiments is designed to gain insight in the dynamical and chemical factors that drive the diurnal variability of the organic aerosol concentration as observed on 7 July 2008 during the OP3 campaign. We draw specific attention to physical and chemical processes that are not routinely taken into account by large-scale models or that are often omitted in the interpretation of measurements. Figure 1 shows the factors that we account for in the interpretation of observed OA, and in this section, we introduce experiments that aim to show the sensitivity of OA formation and concentration to large-scale forcings and several issues related to SOA formation from isoprene.

2.4.1. Large-Scale Meteorological Forcings

[24] With large-scale forcings, we refer to all the meteorological phenomena not directly driven by boundary layer processes. It can encompass mesoscale flows induced by different degrees of surface spatial heterogeneities (from small spatial scale to sea breeze) [*Ouwersloot et al.*, 2011] to phenomena-like subsiding air motions driven by synoptic-scale circulations. We designed two experiments to investigate the influence of large-scale meteorological forcings on the BL dynamics and their subsequent impact on OA. In the first experiment, we analyze the sensitivity of observed OA to subsiding air motions due to divergence of the horizontal wind. In a previous study, *Janssen et al.* [2012] showed that OA concentrations in the BL are sensitive to subsidence, because it suppresses BL growth and enhances entrainment. The subsidence velocity w_s (m s^{-1}) is in our modeling approach represented as follows:

$$w_s = -\omega \cdot h, \tag{2}$$

where ω is the subsidence rate (s^{-1}) and h is the BL height (m). In the sensitivity analysis, we switch subsidence off by

Table 3. The Initial and Boundary Conditions in Boundary Layer (BL) and Free Troposphere (FT) as Obtained From Fitting MXLCH-SOA to the Case Study Observations[a]

Property	Value
Initial BL height h (m)	300
Subsidence rate ω (s^{-1})	$3.0 \cdot 10^{-5}$
Surface sensible heat flux $\overline{w'\theta'}_s$ (K m s^{-1})	$0.30 \sin(\pi t/t_d)$
Entrainment/surface heat-flux ratio $\beta = -\overline{w'\theta'}_e/\overline{w'\theta'}_s$ (dimensionless)	0.2
Initial BL potential temperature $\langle\theta\rangle$ (K)	298
Initial FT potential temperature θ_{FT} (K)	303.5
Potential temperature lapse rate FT γ_θ (K m^{-1})	$0.0030_{h<800m}$ $0.0095_{h\geq 800m}$
Advection of potential temperature A_θ (K m^{-1}))	$-3.0 \cdot 10^{-4}$
Surface latent heat flux $\overline{w'q'}_s$ (g kg^{-1} m s^{-1})	$0.16 \sin(\pi t/t_d)$
Initial BL specific humidity $\langle q\rangle$ (g kg^{-1})	11.5
Initial FT specific humidity q_{FT} (g kg^{-1})	11.4
Specific humidity lapse rate FT γ_q (g kg^{-1} m^{-1})	–0.0026

[a]All initial conditions are imposed at 06:30 LT. Heat fluxes are applied from 06:30 to 14:00 with H = $\rho c_p \overline{w'\theta'}_s$ and LE = $\rho L_v \overline{w'q'}_s$. t is the time (s) and t_d is the length of the day (s). The subscripts s and e indicate values at the surface and the entrainment zone, respectively.

setting ω to 0 and compare it to the base case, as defined in Table 3.

[25] Second, we analyze the sensitivity to advection of heat by the mesoscale flow. The different contributions to heat advection are combined and prescribed to the model as a single advection term (A_θ). The best match with the observations is obtained when this term is negative throughout the day, meaning that relatively cool air is advected (Table 3). In our model setup, we assume that the advection of heat is uniformly distributed within the BL. In the sensitivity analysis, we switch advection of heat off and compare it to the base case.

2.4.2. OH Recycling

[26] In a second sensitivity analysis concerning the sensitivity of OA to chemistry, we evaluate the sensitivity of simulated OA to OH recycling, since this most important oxidant may be underestimated with respect to measurements in high isoprene environments [*Lelieveld et al.*, 2008]. The influence of OH recycling on SOA formation has been accounted for by applying a more detailed chemical mechanism in a global modeling study by *Lin et al.* [2012a]. In that study, it led to decreased SOA yields, because of modifications in the gas-phase oxidation of isoprene. We do not explicitly account for these reaction pathways, but we consider that it can still be useful to include OH recycling to determine how OH concentrations matching the observations affect the formation of terpene SOA (TSOA) for a case study that is well constrained by observational data. In our model, OH recycling is parameterized by applying a variable stoichiometric coefficient n in the reaction of IRO_2 with HO_2 (R20) [*Lelieveld et al.*, 2008; *Vilà-Guerau de Arellano et al.*, 2011]. We compare the base case (no recycling, $n = 0$) with experiments in which n is set to 1 and 2, respectively.

2.4.3. SOA Formation From IEPOX

[27] Under low-NO_x conditions, isoprene epoxydiols (IEPOX) have been found to be important reactive intermediates in the formation of isoprene SOA [*Paulot et al.*, 2009; *Surratt et al.*, 2010; *Lin et al.*, 2012b]. The chemical pathways for SOA formation from IEPOX are not incorporated explicitly in MXLCH-SOA. However, we mimic the catalyzing role of acidic sulfate aerosol on the formation of SOA from IEPOX by incorporating the chemical mechanism suggested by *Paulot et al.* [2009] (see Table 5) and using a fixed aerosol yield of 6.4%, which is the highest yield from experiments by *Lin et al.* [2012b]. In this way, we neglect the complex underlying chemistry, but we obtain a first-order estimation of the magnitude of its effect. In the experiment, the *Paulot et al*. [2009] mechanism replaces the reactions R9 and R20 as used in the default mechanism. In this mechanism, there are some regeneration of OH, but we only evaluate its impact on SOA through IEPOX formation here. So although the implications of OH recycling and IEPOX formation on SOA formation are dealt with in separate sensitivity analyses here, they may be closely linked.

3. Interpretation of Observations by Modeling

[28] We are able to satisfactorily reproduce the dynamics as observed on 7 July 2008 at Bukit Atur, see Figure 4 with initial and boundary conditions as specified in Table 3. The BL height reaching between 800 to 1000 m, as observed by over Borneo from lidar [*Pearson et al.*, 2010] and aircraft measurements [*Robinson et al.*, 2012], appears to be the result of the local surface forcing of the sensible (H) and latent heat flux (LE) with superimposed subsidence and advection. Due to the high H (with a maximum of ~400 W m^{-2}), this low BL height can only be explained when subsidence and advection are accounted for: (1) subsidence directly suppresses the convective motions that are induced by the surface heat flux and (2) advection of relatively cold air cools the BL and consequently increases its potential temperature difference with the FT ($\Delta\theta$), which hinders thermal plumes in breaking through this potential temperature inversion to entrain warm air from the FT. In Figure 1, a typical vertical profile of potential temperature (θ) is sketched to illustrate these effects. These large-scale meteorological forcings may explain the low BL height over Borneo compared to the Amazon, where mixed layer heights typically exceed 1000 m [*Martin et al.*, 1988]. Later, we explicitly investigate the effect of these meteorological forcings on C_{OA}.

[29] The mixed layer potential temperature ($\langle\theta\rangle$) shows a steep increase of 3 K h^{-1} after the heat fluxes become positive, at 06:30. This is caused by direct heating of the BL by the sensible heat flux and by entrainment of warm air during the rapid growth of the BL between 09:00 and 11:30, which are both further enhanced by subsidence. Unfortunately, two observations are missing at 07:30 and 08:00, but the fact that we are able to reproduce the strong gradient in $\langle\theta\rangle$ gives us confidence in the correct representation of its evolution. Specific moisture ($\langle q\rangle$), which initially increases due to the evaporation flux, decreases after 09:30 because

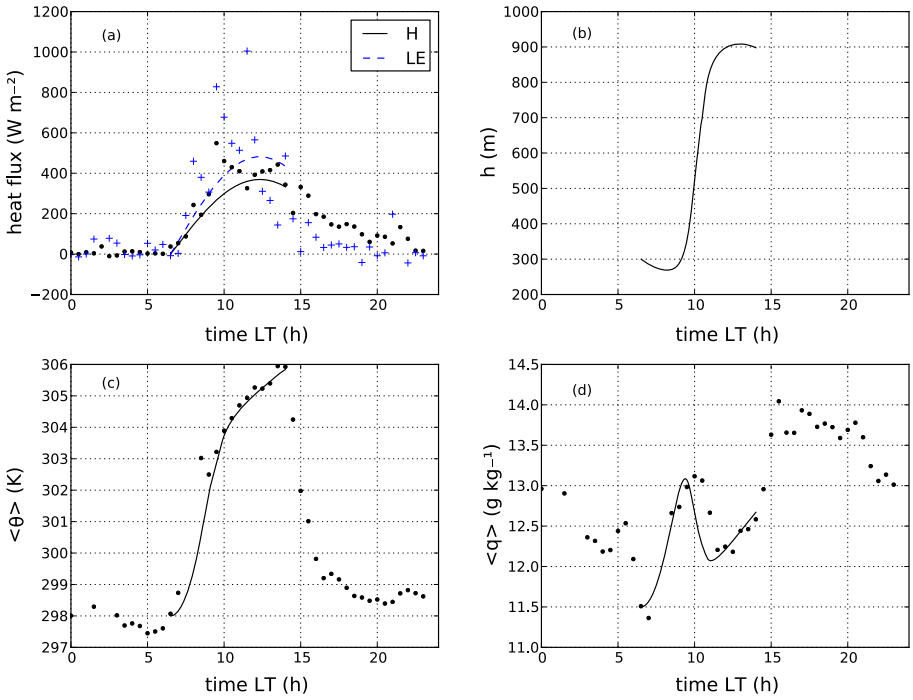

Figure 4. Diurnal evolution of (a) surface sensible (H) and latent (LE) heat flux, which are both prescribed, (b) boundary layer height (h), (c) mixed layer potential temperature ($\langle\theta\rangle$), and (d) mixed layer specific moisture ($\langle q\rangle$) for the case study. Dots indicate tower measurements at 45 m, and model results are indicated by lines.

drier air is entrained during the BL growth and increases again when BL growth ceases around 11:00.

[30] The evolution of the gas-phase species O_3, NO_x, and HO_x is shown in Figure 5 with initial conditions as specified in Table 4. O_3 and NO_x mixing ratios and evolution are reproduced satisfactorily within the bounds set by the scatter in the observations, only $\langle NO_2\rangle$ is overestimated between 09:00 and 11:00. The exact reason for this is unknown, but it may be due to missing chemistry. The crucial point here is that NO concentrations are simulated well, which is needed to calculate the branching of the low- and high-NO_x SOA yields. Our model calculations show that at $\langle NO\rangle \sim 0.1$ ppb, >80% of the terpene and isoprene RO_2 reacts with NO, meaning that we are mostly under the high-NO_x regime. This may, however, not be representative of the pristine tropics, where NO mixing ratios are typically in the order of 10^1 ppt. Note that since HO_2 is overestimated by roughly a factor of 1.5, this is a lower limit for the branching fraction of the high-NO_x channel. Further, it should be noted that we have neglected the $RO_2 + RO_2$ reaction in these calculations, which under the conditions of this study accounts for less than 10% of the RO_2 reactivity. This reaction therefore does not influence the finding that the NO channel dominates over the HO_2 channel. OH is underestimated by a factor of 2–6, depending on considering the lower or the upper bound set by the scatter in the observations. We will discuss possible influences on SOA formation in section 5.2.

[31] Figure 6 shows the diurnal evolution of VOCs and OA. F_{ISO} and F_{TERP} are prescribed and scaled to match the fluxes as observed using the virtual disjunct eddy covariance technique, although it should be noted that these observed fluxes can underestimate the surface flux by 15–20% [*Langford et al.*, 2010]. Temperature-driven terpene emissions may continue during night time and in the early morning, but are much lower than those during day time [*Langford et al.*, 2010] and therefore omitted here. Reasonable agreement is found for mixing ratios of ISO and TERP, which show a similar pattern as specific moisture. An initial increase in their concentrations between 06:30 and 09:30 is followed by a decrease, which is related to the rapid BL growth. In the afternoon, both ⟨ISO⟩ and ⟨TERP⟩ increase again due to continuing emissions and weaker entrainment. The contribution of chemical destruction is rather constant from 09:00 onward, due to a rather constant simulated ⟨OH⟩ (Figure 5). A more thorough budget analysis is given in section 4.

[32] ⟨MVK+MACR⟩ is overestimated between 09:00 and 11:00 by around 0.2 ppb. An overestimation of MVK+MACR was found previously in studies of tropical regions [*Ganzeveld et al.*, 2008; *Pugh et al.*, 2010], and several possible explanations have been proposed, including an underestimation of dry deposition and entrainment of MVK+MACR from the residual layer. The applied deposition velocity (V_d) for MVK+MACR of 2.4 cm s^{-1} as suggested by *Karl et al.* [2010] partly resolves this issue by lowering their concentrations by 15% compared to the case without deposition. Since we set the FT concentration of MVK+MACR to zero, entrainment in this case only dilutes BL concentrations and cannot explain the overestimation. The simplicity of the isoprene oxidation scheme applied here may explain this overestimation. It is relevant to mention that the modeled C_{OA} does not directly depend on ⟨MVK+MACR⟩, since we do not explicitly account for SOA formation from MACR.

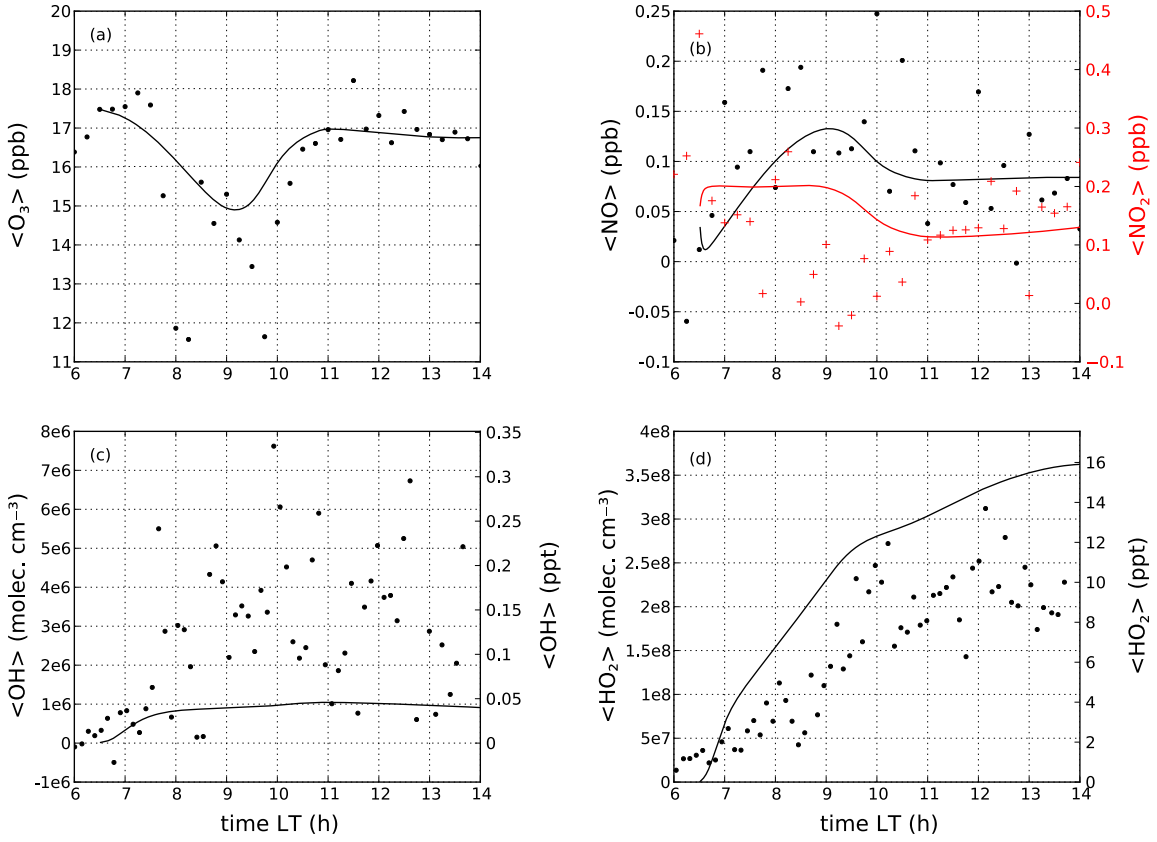

Figure 5. Diurnal evolution of mixed layer concentrations of (a) O_3, (b) OH, and HO_2 (c) NO and (d) NO_2 for the case study. Markers indicate measurements from the tower at 75 m (O_3, NO and NO_2) or 5 m (OH and HO_2).

[33] Both observed and modeled OA concentrations increase during the day, due to SOA formation (Figure 6d). However, the modeled C_{OA} is lower than the observed OOA2, and as the day progresses, this underestimation increases to 60% at the end of the simulation. Possible contributors to this underestimation are a misrepresentation of the pathways leading to ISOA formation or too low OH concentration. These will be subject of the sensitivity analyses in section 5. Also, the high deposition velocity of the SVOCs could cause an underestimation C_{OA}, due to low SOA formation. The simulation with dry deposition of the SVOCs turned off shows the maximum effect of dry deposition of

Table 4. Initial Mixing Ratio in BL and FT and Surface Emission Fluxes of the Reactants as Obtained From Fitting MXLCH-SOA to the Case Study Observations[a]

Species	Initial Mixing Ratio (ppb) BL	FT	Surface Emission/Deposition Flux (ppb m s^{-1})
O_3	17.5	19.0	$-0.45 \sin\left(\frac{\pi t}{t_d}\right)$
NO	0.05	0.0	$9 \cdot 10^{-3}$
NO_2	0.15	0.10	1.5[b]
ISO	0.40	0.0	$0.35 \sin\left(\frac{\pi t}{t_d}\right)$
TERP	0.08	0.0	$0.04 \sin\left(\frac{\pi t}{t_d}\right)$
OA_{BG}	0.60[b]	0.60[b]	0.0
MVK+MACR	0.0	0.0	2.4[c]
TC_i	0.0	0.0	2.4[c]
IC_i	0.0	0.0	2.4[c]
CH_4	1800	1800	0.0
CO	100	100	0.0
O_2	$2 \cdot 10^8$	$2 \cdot 10^8$	0.0
N_2	$8 \cdot 10^8$	$8 \cdot 10^8$	0.0

[a]Species in the reaction mechanism that are not included in this table have zero initial concentrations and zero surface emissions.
[b]$\mu g\ m^{-3}$.
[c]V_d (cm s^{-1}).

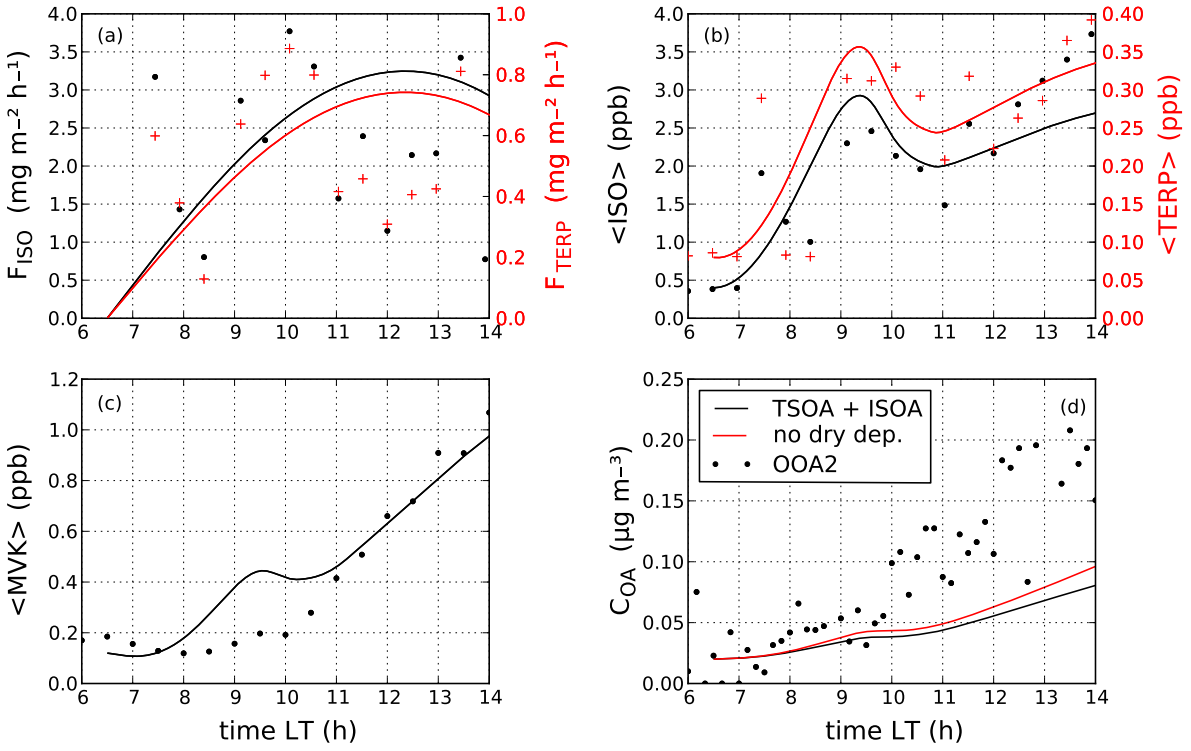

Figure 6. Diurnal evolution of (a) ISO- and TERP-flux, which are both prescribed, and mixed layer concentrations of (b) ISO and TERP, (c) MVK+MACR, and (d) OA for the case study. Markers indicate measurements from the tower at 75 (F_{ISO} and F_{TERP}, ISO, TERP, MVK+MACR) or 33 m (OA).

SVOCs, resulting in a 22% higher C_{OA} at the end of the simulation compared to the case with deposition.

4. Budget Analysis of VOCs, SVOCs, and OA

[34] To understand how dynamics and chemistry interact and how the diurnal evolution of OA results from this interaction, it is useful to analyze the cascade of processes that lead to SOA formation from gas-phase precursors. Here we show the budgets of key species in the formation of OA: VOCs from biogenic emissions, an intermediate semivolatile species SVOC, and OA as their end product, and how these budgets are coupled to the diurnal variability of the boundary layer dynamics.

[35] The budget of a primary VOC reads as follows [*Janssen et al.*, 2012]:

$$\frac{\mathrm{d}\langle \mathrm{VOC}\rangle}{\mathrm{d}t} = \overbrace{\frac{F_{\mathrm{VOC}}}{h}\sin\left(\frac{\pi t}{t_d}\right)}^{\text{emission}} + \overbrace{\frac{w_{\mathrm{e}}\Delta\mathrm{VOC}}{h}}^{\text{entrainment}} - \overbrace{\sum_j k_j\langle \mathrm{VOC}\rangle\langle \mathrm{OX}_j\rangle}^{\text{chemistry}}, \tag{3}$$

where F_{VOC} is the maximum daily VOC emission flux (ppb m s^{-1}), assuming a sinusoidal diurnal emission profile; h is the BL height (m); t is the time since the start of the simulation (s); t_d is the length of the period during which the heat fluxes are positive (s); w_e is the entrainment velocity (m s^{-1}); ΔVOC is the VOC mixing ratio difference (jump) between the BL and the FT (ppb) (with the jump of a scalar or reactant C defined as $\Delta C = C_{FT} - \langle C\rangle$); k_j is the reaction rate of VOC with oxidant OX_j (either O_3 or OH); and $\langle \mathrm{OX}_j\rangle$ is the mixed layer mixing ratio of oxidant OX_j (ppb).

[36] A similar equation holds for SVOCs, but they do not have an emission term and are removed from the atmosphere by dry deposition, so their budget equation is the following:

$$\frac{\mathrm{d}\langle C_{\mathrm{i}}\rangle}{\mathrm{d}t} = \overbrace{\frac{w_{\mathrm{e}}\Delta C_i}{h}}^{\text{entrainment}} + \overbrace{\sum_j \alpha_i k_j\langle \mathrm{VOC}\rangle\langle \mathrm{OX}_j\rangle}^{\text{chemistry}} - \overbrace{\frac{V_{\mathrm{d}Ci}\langle C_i\rangle}{h}}^{\text{deposition}}, \tag{4}$$

where ΔC_i is the concentration jump of the SVOC C_i (ppb), α_i is the stoichiometric coefficient for C_i, and V_{dCi} is its deposition velocity (m s^{-1}).

[37] And finally, the budget of OA reads as follows:

$$\frac{\mathrm{d}\langle OA\rangle}{\mathrm{d}t} = \overbrace{\frac{w_{\mathrm{e}}\Delta \mathrm{OA}_{\mathrm{BG}}}{h}}^{\text{OA}_{\text{BG}}\text{-entrainment}} + \overbrace{\sum_i \left[X_{p,i}\frac{\mathrm{d}C_i}{\mathrm{d}t} + C_i\frac{\mathrm{d}X_{p,i}}{\mathrm{d}t}\right]}^{\text{G/P-partitioning}} - \overbrace{\frac{V_{\mathrm{dOA}}\langle \mathrm{OA}\rangle}{h}}^{\text{deposition}}, \tag{5}$$

where $\Delta \mathrm{OA}_{\mathrm{BG}}$ is the jump in the background organic aerosol concentration between the BL and the FT (µg m^{-3}), and V_{dOA} is the deposition velocity of OA.

[38] In equations (3)–(5), the BL height h modulates the contributions of the emission, entrainment, and deposition terms, and the entrainment velocity w_e appears in the entrainment term. Through the dependence on h and w_e, the evolution of the chemical species is coupled to the dynamics of the boundary layer, which in turn are affected by large-scale meteorological forcings, as will be shown in section 5.1.

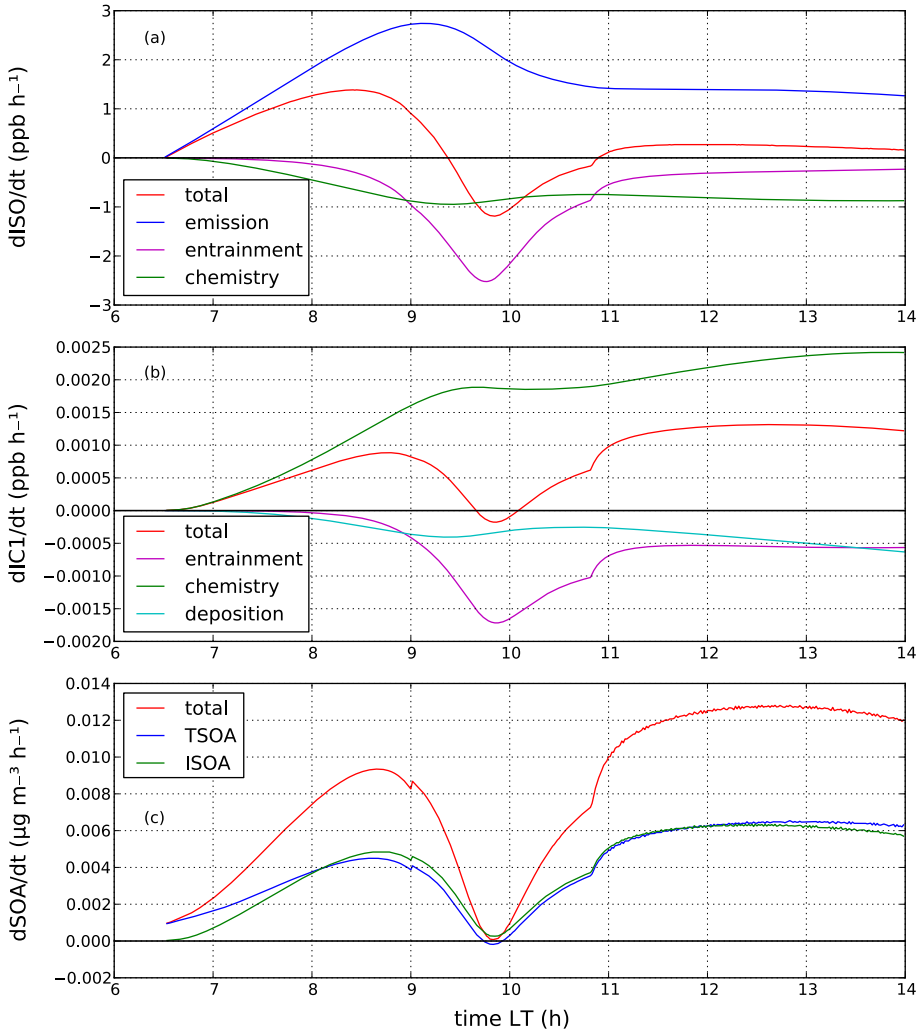

Figure 7. Contribution of the individual processes to the budgets of (a) ISO (equation (3)), (b) the SVOC IC_1, which results from oxidation of ISO (equation (4)), and (c) SOA (equation (5)), split up in the terpene SOA (TSOA) and the isoprene SOA (ISOA) fraction. Note that the contribution of entrainment to the ⟨OA⟩-tendency is zero since the concentrations of OA_{BG} in BL and FT are equal. Therefore, the partitioning of SVOCs from terpenes and isoprene into the aerosol phase forms the only contribution.

[39] Figure 7 shows how the evolution of C_{OA} depends on the behavior of its precursors. The isoprene tendency (Figure 7a), which is shown as an example VOC here, has a positive contribution from the emission term, especially between 08:00 and 10:00 when the emission increases (Figure 6a), and the BL is still shallow as the morning ground inversion is not yet broken. This results in the peak in the isoprene mixing ratio seen in both the observations and model results just before 10:00 (Figure 6b). Entrainment is important during the period of fast BL growth, between 09:00 and 11:00. As shown by the negative value, entrainment contributes to the decrease of isoprene by introducing residual layer/free tropospheric air characterized by lower ISO mixing ratio. Our findings are corroborated by the observed ISO concentration, which decreases between 09:30 and 11:00 (Figure 6b). The chemical destruction term, only by OH in this case, is rather constant from 09:00 onward but becomes the most important loss term after 11:00.

[40] The chemical destruction of isoprene is mirrored in the chemical production of IC_1 (Figure 7b). Due to the low yield of IC_1 (see Table 1), the production of IC_1 is a factor 10^3 smaller than the destruction of ISO. This low yields results in small concentration changes of IC_1 compared to those of ISO. Since the FT concentration is set to zero, the concentration jump is equal to the BL concentration. Therefore, the ratio between entrainment and deposition terms depends solely on the ratio of the entrainment and deposition velocities. w_e peaks at 10:00 at 13 cm s^{-1}, and in our case, the entrainment contribution is larger that of the dry deposition process with V_d =2.4 cm s^{-1}.

[41] The contribution of the entrainment term to the SOA precursors is clearly visible in the evolution of OA (Figure 7c). The budget of OA includes the entrainment of OA_{BG}, but here the concentrations are equal in BL and FT, and therefore, the OA_{BG} entrainment term is zero (first term on the right-hand side (RHS) of equation (5)). This

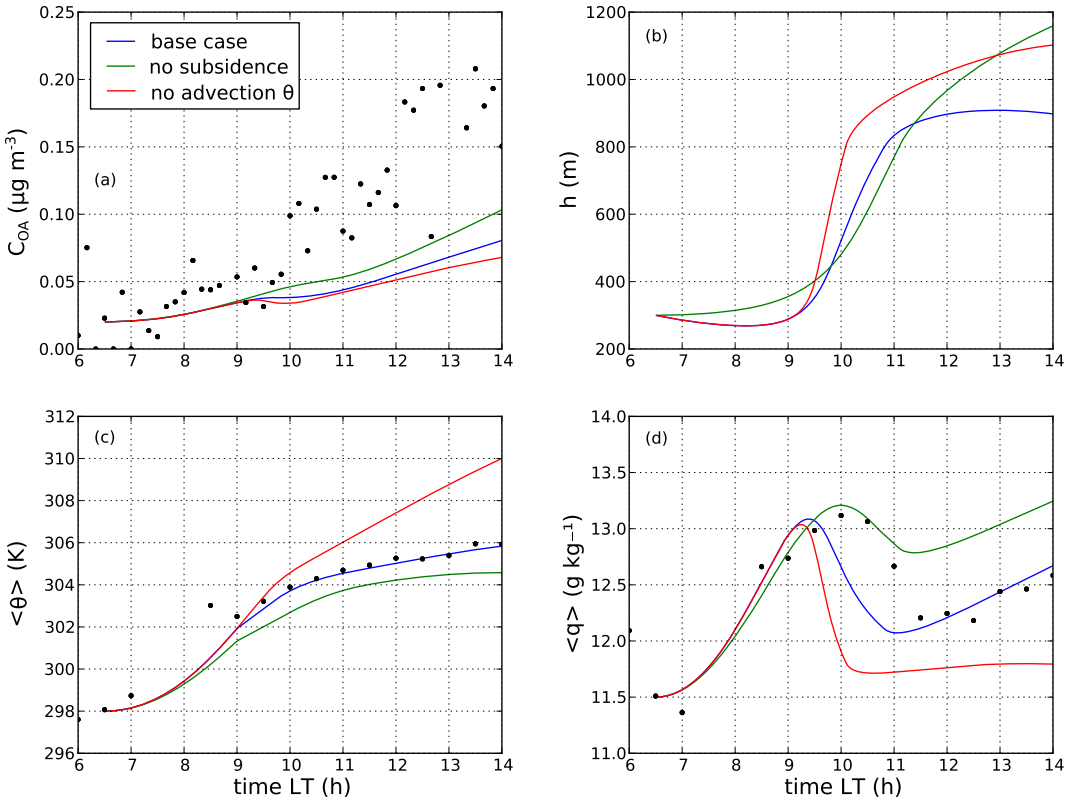

Figure 8. Sensitivity of modeled (a) organic aerosol concentration C_{OA}, (b) BL height h, (c) mixed layer potential temperature $\langle\theta\rangle$, and (d) mixed layer specific humidity $\langle q\rangle$ to subsidence and advection of heat. Shown are the base case (see Table 3), an experiment without subsidence and an experiment with no advection of θ.

is because the OA consists of OA_{BG} and fresh SOA. The former has no concentration gradient between BL and FT, and the latter is calculated at each time step as the fraction of the SVOCs that enter the aerosol phase, in which the effect of entrainment is already accounted for. In case of a large concentration jump of OA_{BG} between BL and FT, the entrainment term is important for the evolution of OA [*Janssen et al.*, 2012]. The minimum in the gas/particle partitioning (second term on the RHS of equation (5)) is therefore caused by the dilution of the SVOCs due to entrainment. The OA tendency has its peak in the afternoon at 12:30, similarly as the SVOC tendency. This is caused not only by the fact that more SVOC is present but also by the presence of a larger available organic mass for SVOCs to partition in. Consequently, partitioning of the SVOCs into the aerosol phase will be efficient, i.e., in equation (1), $X_{p,i}$ increases with increasing C_{OA}. TSOA and ISOA contribute in similar quantities to the calculated SOA formation. ISOA has lower yields than TSOA, but the emission of ISO is a factor of 5 larger than that of TERP, which compensates for this. However, the ISOA shown here should be regarded as a lower limit, and the formation of ISOA through reactive intermediates will be discussed in section 5.3.

[42] We omit advection of any of these species and therefore implicitly assume the footprint area of the site to be horizontally homogeneous for the emission of VOCs, the formation of SVOCs, and the OA concentration. Especially for long-lived species as OA, this assumption may not hold, and we cannot rule out a possible contribution of advection to the OA budget. On the other hand, the satisfactory agreement of the measurements on this particular day and the campaign averages (Figure 2) makes it unlikely that the source of the air masses arriving at the site are of major importance for the diurnal variability.

[43] Another process that has not been taken into account is the dry deposition of OA, as dry deposition of submicron aerosols over forests is not well constrained by observations. Recently, *Farmer et al.* [2013] observed a V_d for the submicron mode mass of 0.02 cm s^{-1} over temperate and tropical forests, which indicates that the contribution of dry deposition would be small. If it would be included, it would act to further increase the discrepancy between measured and modeled OA.

5. Sensitivity Analyses

5.1. Large-Scale Meteorological Forcings

[44] Large-scale meteorological forcings influence the coupled system of BL height (h), mixed layer potential temperature ($\langle\theta\rangle$), and specific moisture ($\langle q\rangle$). Consequently, they affect the OA concentration through their influence on h and w_e, as shown in the previous section. In case of subsidence, the BL growth is suppressed by large-scale downward vertical motions, which lead to a stronger heating of the BL because the same amount of heat is distributed

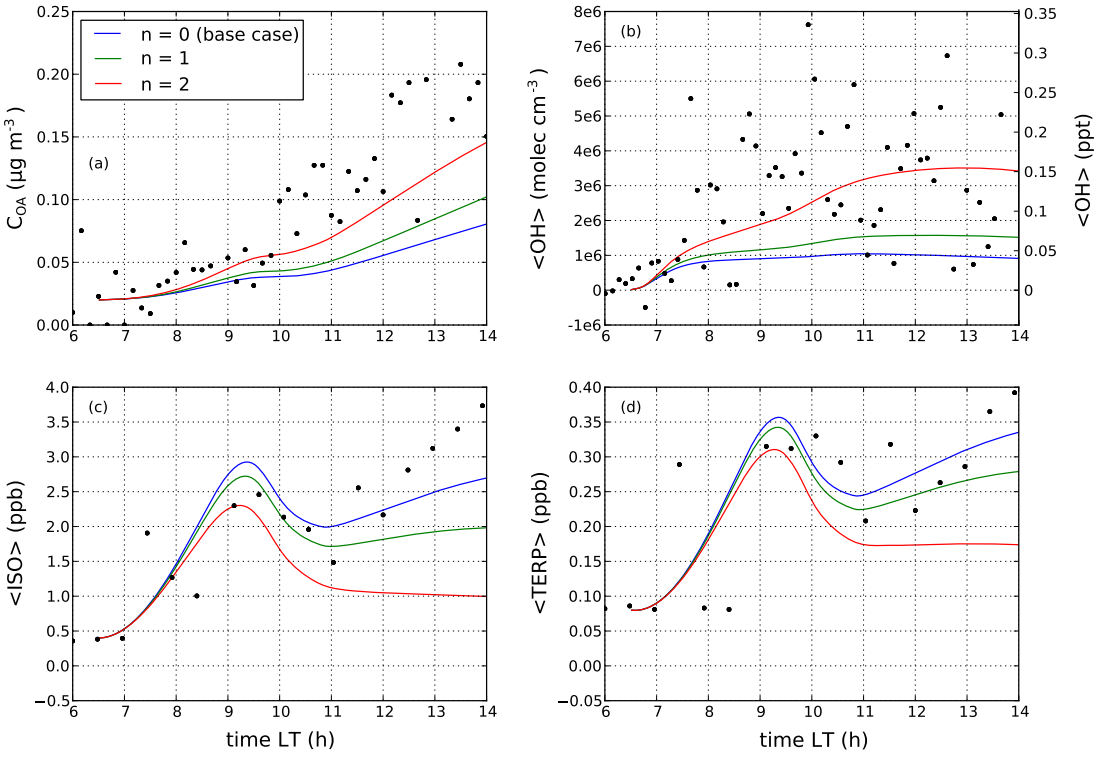

Figure 9. Sensitivity of (a) organic aerosol C_{OA}, (b) OH, (c) ISO, and (d) TERP to OH recycling. Shown are experiments for n = 0, 1, and 2 in R20, respectively.

over a shallower layer. As a consequence, the potential temperature jump at the BL-FT interface decreases, which enhances the entrainment velocity [*Janssen et al.*, 2012]. In our case study, not taking subsidence into account would have led to an overestimation of h of 250 m at the end of the numerical experiment (Figure 8), an underestimation of $\langle\theta\rangle$ by 1.5 K and a BL which is too moist. Because of the increased entrainment velocity, OA is diluted more under the presence of subsidence, resulting in 27% lower OA at the end of the simulation.

[45] Advection of θ in this case acts to cool the BL. Therefore, the potential temperature jump across the BL-FT interface increases, which weakens entrainment (so opposite to the effect of subsidence) and BL growth. Not taking advection of cool air into account results in a BL which is 200 m higher at the end of the run than in the case with advection (similar as for subsidence), an overestimation of $\langle\theta\rangle$ by 4 K and an underestimation of $\langle q\rangle$ by 0.9 g kg^{-1}. Due to the weaker entrainment when advection of cool air is considered, the OA precursors are diluted less, leading to more SOA formation and a 16% higher C_{OA} in the case with advection (Figure 8).

[46] Subsidence and advection of cold air, while both decreasing BL height, therefore have opposing effects on C_{OA}.

5.2. OH Recycling

[47] The evolution of OA has so far been simulated in this paper without considering OH recycling from isoprene (n = 0 in R20). In this section, we explore n = 1 and n = 2 in R20. This corresponds to daily average recycling rates of OH with respect to the OH consumed by the first-step oxidation of isoprene of 19% and 54%, respectively, which is below the range of 75% to 120%, as estimated recently by *Taraborrelli et al.* [2012]. Nevertheless, including OH recycling leads to a better agreement with the observations of $\langle$OH$\rangle$, especially for n = 2 (Figure 9). This enhancement of $\langle$OH$\rangle$ leads to an increase of the calculated C_{OA} at the end of the simulation by 25% and 75% for n = 1 and n = 2, respectively. This enhancement of the calculated C_{OA}, however, is not enough to explain the observed OOA2. On the other hand and as expected from reactions R9 and R30, ISO and TERP are depleted at a faster rate when OH is recycled, which leads to an underestimation of their concentrations as n is increased, especially in the afternoon when isoprene oxidation and OH recycling have a maximum. This is similar to the findings of *Pugh et al.* [2010] for observations made during OP3 I. They questioned the validity of the assumption of a well-mixed layer and suggested that the segregation of isoprene into distinct plumes could deplete OH in those plumes, which may have affected the measurements. However, the high degree of segregation assumed in their simulations of this effect (50%) was later dispelled by *Pugh et al.* [2011] and *Ouwersloot et al.* [2011], who found a reduction of the rate constant of the isoprene and OH reaction due to incomplete mixing of less than 15%. Moreover, in search of missing OH sources, *Whalley et al.* [2011] included the isoprene + O_3 reaction, but OH production from this reaction was not found to be a major missing term in the OH budget under the low O_3 concentrations during the OP3 campaign. Also, they concluded that terpene concentrations were too low to provide the missing OH source.

[48] The main point here is that we are able to reproduce the evolution of ISO and TERP satisfactorily for n = 0 as

Table 5. *Paulot et al.* [2009] Mechanism for Oxidation of Isoprene Under Low-NO_x Conditions, Which Replaces R9 and R20 in Table 1 in the Sensitivity Analysis for the Chemical Mechanism of SOA Formation From Isoprene (Section 5.3)

R29	ISO + OH	→	IRO_2	$2.70 \cdot 10^{-11} \cdot e^{\frac{390}{T}}$
R30	IRO_2 + HO_2	→	0.880 ISOPOOH + 0.120 OH + 0.047 MACR + 0.073 MVK + 0.120 HO_2 + 0.120 CH_2O	$7.40 \cdot 10^{-13} \cdot e^{\frac{700}{T}}$
R31	ISOPOOH + OH	→	IEPOX + OH	$1.90 \cdot 10^{-11} \cdot e^{\frac{390}{T}}$
R32	ISOPOOH + OH	→	0.70 ISOPOO + 0.300 HC_5 + 0.300 OH	$3.80 \cdot 10^{-12} \cdot e^{\frac{200}{T}}$
R33	IEPOX + OH	→	IEPOXOO	$5.78 \cdot 10^{-11} \cdot e^{\frac{-400}{T}}$
R34	IEPOXOO + HO_2	→	0.725 HAC + 0.275 GLYC + 0.275 GLYX + 0.275 MGLY + 1.125 OH + 0.825 HO_2 + 0.200 CO_2 + 0.375 CH_2O + 0.074 HCOOH + 0.251 CO	$7.40 \cdot 10^{-13} \cdot e^{\frac{700}{T}}$

a function of emission, entrainment, and chemistry. Hereby, the emissions are constrained by the flux measurements, and the correct representation of BL dynamics gives us confidence in the representation of entrainment. Seen in this way, the first-step oxidation by OH (and O_3 in case of TERP) is apparently represented reasonably well in the base case. So while increasing n leads to an improved representation of ⟨OH⟩ and C_{OA}, it serves to worsen the match with the observed ⟨TERP⟩ and ⟨ISO⟩. OH recycling thus has the potential to influence modeled SOA formation in high isoprene environments, but current knowledge is not sufficient to constrain its effects.

5.3. SOA Formation From IEPOX

[49] Our last sensitivity study focuses on the formation of IEPOX SOA, catalyzed by acidic sulfate aerosol (Table 5). We find concentrations of IEPOX in the order of $\sim 10^{-1}$ ppb after midday (Figure 10a), which is of the same order of magnitude as calculated by a global model for Borneo [*Paulot et al.*, 2009]. The branching between the IRO_2 + HO_2 and the IRO_2 + NO reactions determines the efficiency with which IEPOX is formed. As in the previous experiments, the NO channel dominates, with the HO_2 channel contributing only ∼13% to the destruction of IRO_2.

[50] IEPOX SOA is modeled here with a fixed yield of 6.4%, which is the largest yield found in the experiments of *Lin et al.* [2012b]. 82Fac shows a decrease, possibly due to entrainment, from 08:00 to 09:00 and after that time increases rapidly to reach a concentration which is 1 order of magnitude greater at 14:00 than its minimum at 09:00 (Figure 10b). We are not able to match the strong increase of 82Fac as observed between 09:00 and 14:00. An IEPOX SOA yield of 35% would be required to explain this rapid increase.

[51] There are several possible causes for the underestimation of the concentration of 82Fac by the model. First, the concentration of gas-phase IEPOX may be underestimated, but unfortunately, there is no data available to validate this. Further, we employ a fixed yield of IEPOX SOA, which implies that effects of the OA_{BG} on gas/particle partitioning are not accounted for, which may affect the aerosol yield of semivolatile species (see equation (1)). Then, the yield of IEPOX SOA found in chamber studies [*Lin et al.*, 2012b] may be too low, possibly due to yet unknown chemical pathways. Finally, we consider a meteorological factor, long range horizontal transport by advection. Advection may be important because OA has, in contrast to VOCs, a long atmospheric lifetime of days to a week. This means that observed OA could reflect integrated VOC oxidation over a larger area and period rather than in situ production of OA from VOCs. As a consequence, it is plausible that IEPOX SOA is advected to the measurement site that is formed from isoprene emitted at the oil palm plantations located 50 km and further to the South-East, which emit 4–7 times more isoprene than the forest [*Hewitt et al.*, 2010]. However, it is not known what the 82Fac looks like after aging, and it

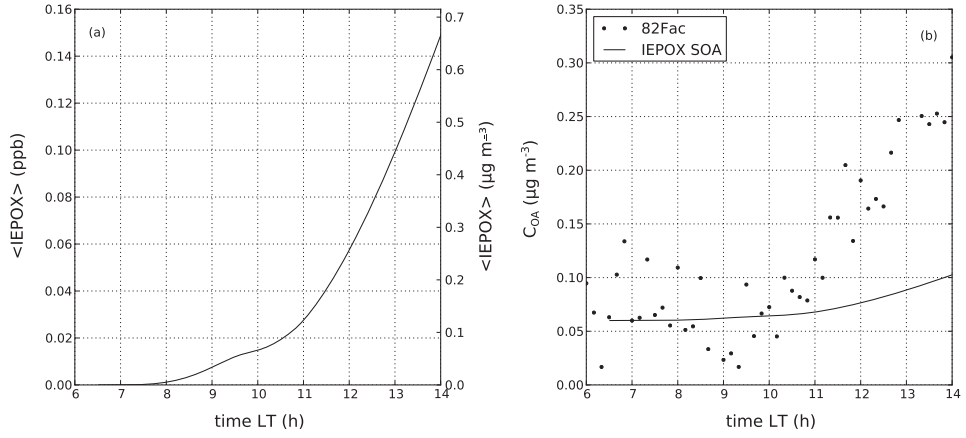

Figure 10. Concentration of (a) IEPOX and (b) IEPOX SOA, assuming a fixed yield for the latter of 6.4%, which is the upper limit under acidic conditions found by *Lin et al.* [2012b].

could be transformed into OOA2 or OOA1 by the time it reaches the site. Although we cannot rule out the contribution of advection, there are two reasons to expect that the fast increase of 82Fac is likely not due to advection. First, the fact that 82Fac was not observed in morning air plane profiles, but that it was observed in the afternoon flights, may indicate that the 82Fac is formed rapidly and mainly from local sources. Second, the time at which the fast increase of 82Fac begins (after 10:00, see Figure 10b) corresponds well with the modeled increase of IEPOX and IEPOX SOA.

6. Conclusions

[52] We studied the diurnal evolution of organic aerosol, its gas-phase precursors, and their oxidants coupled to the dynamics of a convective boundary layer for a characteristic situation observed above the tropical forest during the OP3 field campaign. Observations of BL dynamics and chemical species combined with a boundary layer model of physics and chemistry are used to determine the dominant processes in the SOA formation driven by terpene and isoprene emissions. We are able to satisfactorily reproduce the diurnal variability of the BL in terms of its height, potential temperature, and specific humidity as driven by land surface and large-scale meteorological forcings. Advection of cooler air and subsidence are important contributions to the characterization of the BL as observed over Borneo and complicate the characterization of a tropical BL climatology. Because of their influence on BL height and entrainment, subsidence and advection of heat affect the diurnal evolution of chemical species in the BL and should be taken into account when interpreting observations of OA. Subsidence and advection of cool air, while both decreasing BL height, have opposing effects on the diurnal trend of C_{OA}.

[53] An analysis of the budgets of VOCs, SVOCs, and OA shows the importance of studying dynamical and chemical processes simultaneously in order to understand the diurnal variability of reactants. Specifically, it shows how the OA budget is strongly modified by the various processes that shape the diurnal cycle of its gas-phase precursors, in which the signal of entrainment is clearly visible.

[54] By confronting our model with a rather complete set of data of gas-phase chemistry and organic aerosol, we are able to exclude the influence of some factors that in other studies have been suggested to explain underestimation by models of biogenic OA concentrations. Nevertheless, as in previous studies, we underestimate OA concentrations by about a factor of 2, even though we are able to reproduce the diurnal evolution of isoprene and terpene concentrations with observed and prescribed fluxes and we explicitly take the role of entrainment on VOCs and their oxidants into account.

[55] In our investigation of the role of isoprene chemistry in SOA formation, we find that OH recycling decreases the model-measurement discrepancy of OA concentrations, but at the cost of a worse comparison with VOC concentrations. Before isoprene SOA formation can be quantified, OH recycling must be understood. In spite of the incorporation of a parameterization based on the current knowledge on the formation of IEPOX SOA in our model, we underestimate the concentration of 82Fac, an OA component thought to be specifically related to SOA from isoprene epoxides (IEPOX). There are several factors which may explain this underestimation, and further insights in the formation and evolution in the atmosphere of IEPOX SOA are needed to get a definitive answer. We find that the low-NO_x pathway leading to IEPOX formation is only a minor one under observed NO concentrations. Nevertheless, the concentration of 82Fac is of comparable magnitude as that of OOA2, suggesting that a minor pathway in the gas-phase chemistry of isoprene can still lead to substantial SOA formation.

[56] The strong dependence of isoprene SOA formation on NO_x chemistry implies that if NO concentrations increase in Borneo by increased anthropogenic activities, the type and amount of isoprene SOA has the potential to change significantly.

[57] Although incorporating these new pathways does not yet explain the discrepancies between modeled and observed biogenic OA, we propose that models need to account for the different pathways by which isoprene chemistry drives SOA formation, both through formation of its second-generation products following the low- and high-NO_x pathways and through its effect on gas-phase chemistry by OH recycling.

[58] Since our model includes only SOA-forming species resulting from the first-step oxidation of isoprene and terpenes, there may be additional sources of SOA, for instance, higher generation oxidation products or unmeasured very reactive species that contribute to the OA budget at the studied site and that should be taken into account in future studies in order to close the budget.

[59] Finally, we advocate the use of conceptual but realistic models similar to the one presented here to bridge the gap between observations made during chamber studies and field campaigns, on one hand, and the gap between local observations and large-scale forcings, on the other hand, to gain further understanding of the organic aerosol budget in tropical forests.

[60] **Acknowledgments.** We thank three anonymous referees for their valuable comments on the manuscript. J.L.J. was supported by NSF ATM-0919189 and DOE (BER/ASR program) DE-SC0006035/DE-SC0006711. TAMP thanks COST action ES0804 for funding a visit to Wageningen UR. The University of Manchester activities were supported by the UK Natural Environment Research Council (NERC) through a PhD studentship (NHR) and the project Oxidant and particle photochemical processes above a South-East Asian tropical rain forest (OP3) [grant ref: NE/D004624/1].

References

Bessagnet, B., C. Seigneur, and L. Menut (2010), Impact of dry deposition of semi-volatile organic compounds on secondary organic aerosols, *Atmos. Environ.*, *44*, 1781–1787, doi:10.1016/j.atmosenv.2010.01.027.

Capes, G., J. G. Murphy, C. E. Reeves, J. B. McQuaid, J. F. Hamilton, J. R. Hopkins, J. Crosier, P. I. Williams, and H. Coe (2009), Secondary organic aerosol from biogenic VOCs over West Africa during AMMA, *Atmos. Chem. Phys.*, *9*, 3841–3850, doi:10.5194/acp-9-3841-2009.

Carlton, A. G., C. Wiedinmyer, and J. H. Kroll (2009), A review of Secondary Organic Aerosol (SOA) formation from isoprene, *Atmos. Chem. Phys.*, *9*, 4987–5005, doi:10.5194/acp-9-4987-2009.

Chan, A. W. H., M. N. Chan, J. D. Surratt, P. S. Chhabra, C. L. Loza, J. D. Crounse, L. D. Yee, R. C. Flagan, P. O. Wennberg, and J. H. Seinfeld (2010), Role of aldehyde chemistry and NO_x concentrations in secondary organic aerosol formation, *Atmos. Chem. Phys.*, *10*, 7169–7188, doi:10.5194/acp-10-7169-2010.

Chen, Q., et al. (2009), Mass spectral characterization of submicron biogenic organic particles in the Amazon Basin, *Geophys. Res. Lett.*, *36*, L20806, doi:10.1029/2009GL039880.

Donahue, N. M., A. L. Robinson, C. O. Stanier, and S. N. Pandis (2006), Coupled partitioning, dilution, and chemical aging of semivolatile organics, *Environ. Sci. Technol.*, *40*, 2635–2643, doi:10.1021/es052297c.

Farmer, D., Q. Chen, J. Kimmel, K. Docherty, E. Nemitz, P. Artaxo, C. Cappa, S. Martin, and J. Jimenez (2013), Chemically-resolved particle fluxes over tropical and temperate forests, *Aerosol Sci. Technol.*, *47*(7), 818–830, doi:10.1080/02786826.2013.791022.

Ganzeveld, L., et al. (2008), Surface and boundary layer exchanges of volatile organic compounds, nitrogen oxides and ozone during the GABRIEL campaign, *Atmos. Chem. Phys.*, *8*, 6223–6243, doi:10.5194/acpd-8-11909-2008.

Hewitt, C. N., et al. (2010), Overview: Oxidant and particle photochemical processes above a south-east Asian tropical rainforest (the OP3 project): Introduction, rationale, location characteristics and tools, *Atmos. Chem. Phys.*, *10*, 169–199, doi:10.5194/acp-10-169-2010.

Janssen, R. H. H., J. Vilà-Guerau de Arellano, L. N. Ganzeveld, P. Kabat, J. L. Jimenez, D. K. Farmer, C. C. van Heerwaarden, and I. Mammarella (2012), Combined effects of surface conditions, boundary layer dynamics and chemistry on diurnal SOA evolution, *Atmos. Chem. Phys.*, *12*, 6827–6843, doi:10.5194/acp-12-6827-2012.

Karl, T., A. Guenther, R. J. Yokelson, J. Greenberg, M. Potosnak, D. R. Blake, and P. Artaxo (2007), The tropical forest and fire emissions experiment: Emission, chemistry, and transport of biogenic volatile organic compounds in the lower atmosphere over Amazonia, *J. Geophys. Res.*, *112*, D18302, doi:10.1029/2007JD008539.

Karl, T., A. Guenther, A. Turnipseed, G. Tyndall, P. Artaxo, and S. Martin (2009), Rapid formation of isoprene photo-oxidation products observed in Amazonia, *Atmos. Chem. Phys.*, *9*, 7753–7767, doi:10.5194/acp-9-7753-2009.

Karl, T., P. Harley, L. Emmons, B. Thornton, A. Guenther, C. Basu, A. Turnipseed, and K. Jardine (2010), Efficient atmospheric cleansing of oxidized organic trace gases by vegetation, *Science*, *330*, 816–819, doi:10.1126/science.1192534.

Kjaergaard, H. G., H. C. Knap, K. B. Ornso, S. Jorgensen, J. D. Crounse, F. Paulot, and P. O. Wennberg (2012), Atmospheric fate of methacrolein. 2. Formation of lactone and implications for organic aerosol production, *J. Phys. Chem. A*, *116*, 5763–5768, doi:10.1021/jp210853h.

Kroll, J. H., N. L. Ng, S. M. Murphy, R. C. Flagan, and J. H. Seinfeld (2006), Secondary organic aerosol formation from isoprene photooxidation, *Environ. Sci. Technol.*, *40*, 1869–1877, doi:10.1021/es0524301.

Lane, T. E., N. M. Donahue, and S. N. Pandis (2008), Effect of NO_x on secondary organic aerosol concentrations, *Environ. Sci. Technol.*, *42*, 6022–6027, doi:10.1021/es703225a.

Langford, B., P. K. Misztal, E. Nemitz, B. Davison, C. Helfter, T. A. M. Pugh, A. R. MacKenzie, S. F. Lim, and C. N. Hewitt (2010), Fluxes and concentrations of volatile organic compounds from a South-East Asian tropical rainforest, *Atmos. Chem. Phys.*, *10*, 8391–8412, doi:10.5194/acp-10-8391-2010.

Lelieveld, J., et al. (2008), Atmospheric oxidation capacity sustained by a tropical forest, *Nature*, *452*, 737–740, doi:10.1038/nature06870.

Lilly, D. K. (1968), Models of cloud-topped mixed layers under a strong inversion, *Q. J. Roy. Meteor. Soc.*, *94*, 292–309.

Lin, G., J. E. Penner, S. Sillman, D. Taraborrelli, and J. Lelieveld (2012a), Global modeling of SOA formation from dicarbonyls, epoxides, organic nitrates and peroxides, *Atmos. Chem. Phys.*, *12*, 4743–4774, doi:10.5194/acp-12-4743-2012.

Lin, Y.-H., et al. (2012b), Isoprene epoxydiols as precursors to secondary organic aerosol formation: Acid-catalyzed reactive uptake studies with authentic compounds, *Environ. Sci. Technol.*, *46*, 250–258, doi:10.1021/es202554c.

Mao, J., et al. (2012), Insights into hydroxyl measurements and atmospheric oxidation in a California forest, *Atmos. Chem. Phys.*, *12*, 8009–8020, doi:10.5194/acp-12-8009-2012.

Martin, C. L., D. Fitzjarrald, M. Garstang, A. P. Oliveira, S. Greco, and E. Browell (1988), Structure and growth of the mixing layer over the Amazonian rain forest, *J. Geophys. Res.*, *93*, 1361–1375, doi:10.1029/JD093iD02p01361.

Ouwersloot, H. G., J. Vilà-Guerau de Arellano, C. C. van Heerwaarden, L. N. Ganzeveld, M. C. Krol, and J. Lelieveld (2011), On the segregation of chemical species in a clear boundary layer over heterogeneous land surfaces, *Atmos. Chem. Phys.*, *11*, 10,681–10,704, doi:10.5194/acp-11-10681-2011.

Ouwersloot, H. G., J. Vilà-Guerau de Arellano, A. C. Nölscher, M. C. Krol, L. N. Ganzeveld, C. Breitenberger, I. Mammarella, J. Williams, and J. Lelieveld (2012), Characterization of a boreal convective boundary layer and its impact on atmospheric chemistry during HUMPPA-COPEC-2010, *Atmos. Chem. Phys.*, *12*, 9335–9353, doi:10.5194/acp-12-9335-2012.

Paulot, F., J. D. Crounse, H. G. Kjaergaard, A. Kürten, J. M. St. Clair, J. H. Seinfeld, and P. O. Wennberg (2009), Unexpected epoxide formation in the gas-phase photooxidation of isoprene, *Science*, *325*, 730–733, doi:10.1126/science.1172910.

Pearson, G., F. Davies, and C. Collier (2010), Remote sensing of the tropical rain forest boundary layer using pulsed Doppler lidar, *Atmos. Chem. Phys.*, *10*, 5891–5901, doi:10.5194/acp-10-5891-2010.

Pugh, T. A. M., et al. (2010), Simulating atmospheric composition over a South-East Asian tropical rainforest: Performance of a chemistry box model, *Atmos. Chem. Phys.*, *10*, 279–298, doi:10.5194/acp-10-279-2010.

Pugh, T. A. M., A. R. MacKenzie, B. Langford, E. Nemitz, P. K. Misztal, and C. N. Hewitt (2011), The influence of small-scale variations in isoprene concentrations on atmospheric chemistry over a tropical rainforest, *Atmos. Chem. Phys.*, *11*, 4121–4134, doi:10.5194/acp-11-4121-2011.

Robinson, N. H., et al. (2011a), Evidence for a significant proportion of Secondary Organic Aerosol from isoprene above a maritime tropical forest, *Atmos. Chem. Phys.*, *11*, 1039–1050, doi:10.5194/acp-11-1039-2011.

Robinson, N. H., et al. (2011b), Source attribution of Bornean air masses by back trajectory analysis during the OP3 project, *Atmos. Chem. Phys.*, *11*, 9605–9630, doi:10.5194/acp-11-9605-2011.

Robinson, N. H., J. D. Allan, J. A. Trembath, P. D. Rosenberg, G. Allen, and H. Coe (2012), The lofting of Western Pacific regional aerosol by island thermodynamics as observed around Borneo, *Atmos. Chem. Phys.*, *12*, 5963–5983, doi:10.5194/acp-12-5963-2012.

Sjostedt, S. J., J. G. Slowik, J. R. Brook, R. Y.-W. Chang, C. Mihele, C. A. Stroud, A. Vlasenko, and J. P. D. Abbatt (2011), Diurnally resolved particulate and VOC measurements at a rural site: Indication of significant biogenic secondary organic aerosol formation, *Atmos. Chem. Phys.*, *11*, 5745–5760, doi:10.5194/acp-11-5745-2011.

Slowik, J. G., et al. (2010), Characterization of a large biogenic secondary organic aerosol event from eastern Canadian forests, *Atmos. Chem. Phys.*, *10*, 2825–2845, doi:10.5194/acp-10-2825-2010.

Stone, D., et al. (2011), Isoprene oxidation mechanisms: Measurements and modelling of OH and HO_2 over a South-East Asian tropical rainforest during the OP3 field campaign, *Atmos. Chem. Phys.*, *11*, 6749–6771, doi:10.5194/acp-11-6749-2011.

Surratt, J. D., A. W. H. Chan, N. C. Eddingsaas, M. Chan, C. L. Loza, A. J. Kwan, S. P. Hersey, R. C. Flagan, P. O. Wennberg, and J. H. Seinfeld (2010), Reactive intermediates revealed in secondary organic aerosol formation from isoprene, *Proc. Nat. Acad. Sci.*, *107*, 6640–6645, doi:10.1073/pnas.0911114107.

Taraborrelli, D., M. G. Lawrence, J. N. Crowley, T. J. Dillon, S. Gromov, C. B. M. Grosz, L. Vereecken, and J. Lelieveld (2012), Hydroxyl radical buffered by isoprene oxidation over tropical forests, *Nat. Geosci.*, *5*, 190–193, doi:10.1038/ngeo1405.

Tennekes, H. (1973), A model for the dynamics of the inversion above a convective boundary layer, *J. Atmos. Sci.*, *30*, 558–567, doi:10.1175/1520-0469(1973)030<0558:AMFTDO>2.0.CO;2.

Thunis, P., and R. Bornstein (1996), Hierarchy of mesoscale flow assumptions and equations, *J. Atmos. Sci.*, *53*, 380–397, doi:10.1175/1520-0469(1996)053<0380:HOMFAA>2.0.CO;2.

Tsimpidi, A. P., V. A. Karydis, M. Zavala, W. Lei, L. Molina, I. M. Ulbrich, J. L. Jimenez, and S. N. Pandis (2010), Evaluation of the volatility basis-set approach for the simulation of organic aerosol formation in the Mexico City metropolitan area, *Atmos. Chem. Phys.*, *10*, 525–546, doi:10.5194/acp-10-525-2010.

Vilà-Guerau de Arellano, J., K. van den Dries, and D. Pino (2009), On inferring isoprene emission surface flux from atmospheric boundary layer concentration measurements, *Atmos. Chem. Phys.*, *9*, 3629–3640, doi:10.5194/acp-9-3629-2009.

Vilà-Guerau de Arellano, J., E. G. Patton, T. Karl, K. van den Dries, M. C. Barth, and J. J. Orlando (2011), The role of boundary layer dynamics on the diurnal evolution of isoprene and the hydroxyl radical over tropical forests, *J. Geophys. Res.*, *116*, D07304, doi:10.1029/2010JD014857.

Whalley, L. K., et al. (2011), Quantifying the magnitude of a missing hydroxyl radical source in a tropical rainforest, *Atmos. Chem. Phys.*, *11*, 7223–7233, doi:10.5194/acp-11-7223-2011.